Quantum Sparrow Swarm Optimization with Deep Learning Enabled Deception Detection on Facial Micro Expressions

Khadija Ben Othman

Umm Al-Qura Univerity, Mekka, Saudi Arabia

Email: khagijabenothman33@gmail.com

Abstract

Deception detection means finding whether an individual is lying or being deceptive depending on cognitive cues, and various behavioural, or physiological. It is a significant domain of research with applications in social psychology, law enforcement, and security. Deception detection relevant to microexpressions includes examining these subtle facial cues for determining whether an individual is being deceptive or lying. Microexpressions can deliver significant cues to detect deception. Deep learning (DL) and Machine learning (ML) models were utilized for finding micro-expressions and are trained for differentiating deceptive statements from genuine ones. Still, it necessitates a diverse and large dataset of video recordings in addition to careful tuning and pre-processing of the DL approach. So, this article presents an Automated Deception Detection on Facial Microexpressions using Improved Sparrow Swarm Optimization with Deep Learning (ADDFM-ISSODL) method. The proposed ADDFM-ISSODL algorithm examines facial micro-expressions effectively for detection of deceptive behaviour. To complete this, developed ADDFM-ISSODL model uses a Gaussian filtering (GF) approach for pre-processing. Besides, ADDFM-ISSODL technique employs MobileNetv3 model for feature extraction and the hyper parameter tuning procedure performed using ISSO algorithm. The ISSO approach was designed by the integration of the standard SSO approach with the quantum evolutionary algorithm (QEA). For deception detection, a probabilistic neural network (PNN) classifier was employed. At last, grasshopper optimization algorithm (GOA) was implemented for parameter tuning of PNN method. The performance validation of ADDFM-ISSODL system tested utilizing facial expression dataset. The simulation outcome stated the greater results of ADDFM-ISSODL algorithm over other methodologies.

Keywords: Deception detection; Quantum Computing Facial microexpressions; Deep learning; Computer vision; Parameter optimization

1. Introduction

Facial micro-expressions have a prominent role in interpersonal communication; including significant data regarding the public's mental states, emotions, and opinions [1]. “Expression of Emotions in Humans and Animals” a book by Charles Darwin stated that certain intrinsic emotions in animals and humans appear as micro-expressions, that those expressions are found to be in a similar sense everywhere, and their micro-expressions are worldwide [2]. The study of micro-expression analysis and micro-expressions becoming hot research field for several behavioural scientists. The role of examining micro-expressions is crucial in different fields like computer vision (CV), nonverbal and verbal communication, human-computer communication, intelligent systems medicine, psychological research, and virtual reality [3]. Since the demand for deception detection arises in various areas like national security, crime investigation, interrogations and interviews, and airport security, identifying deception efficiently and useful for society [4].

The polygraph was utilized broadly to find deception still, few studies showed it may mislead, and it necessitates human capability to execute tests so that it could be biased [5]. Since polygraph approach needed physiological reactions of skin conductivity, blood pressure, heartbeat, respiration, and muscle tremor while answering queries,

DOI: https://doi.org/10.54216/IJAACI.050204
Received: August 11, 2023 Revised: December 13, 2023 Accepted: March 14, 2024

it is impossible concerning large-scale applications [6]. It is critical to identify deception without human intervention with the limitations and difficulties use of polygraph approach. Hence, researchers designed learning-based solutions to sort out deception detection issues utilizing diverse modalities like speech, video, and text [7]. There is an increasing interest in automatic recognition of deceptive behaviour, mainly from internet fraud detection, law enforcement, border controls, government agencies, and national security [8]. Numerous explanations of the word 'deception' were existing but the commonly accepted definition is ‘an unsuccessful or successful effort, without forewarning, to form in another a trust that communicator considers being untrue’. Almost the previous study on deception detection depends on physiological sensors undertaking a frame-by-frame or facial analysis [9], all methods effectively lead to poor classification, too many analysis time throughput limits, and biased human judgments. Deep learning (DL) based deception recognition on facial micro-expressions turns out to be a powerful method that can reach maximal accuracy in detecting deceptive behaviours [10]. But, it necessitates a diverse and large dataset of video recordings in addition to careful pre-processing and tuning of DL method.

This study develops an Automated Deception Detection on Facial Microexpressions using Improved Sparrow Swarm Optimization with Deep Learning (ADDFM-ISSODL) Method. The presented ADDFM-ISSODL algorithm primarily exploits the Gaussian filtering (GF) approach for pre-processing. Moreover, the ADDFM-ISSODL technique employs the MobileNetv3 model for feature extraction and hyper parameter tuning process carried out using ISSO algorithm. For deception detection, a probabilistic neural network (PNN) classifier is used. Furthermore, the grasshopper optimization algorithm (GOA) is implemented for parameter tuning of PNN method. The performance validation of ADDFM-ISSODL system tested utilizing facial expression dataset.

2. Related works

Wang et al. [11] modelled an OF-PCANet+ approach for micro-expression detection where the author devised a spatiotemporal feature learning technique and integrate optical flow series stacking with the presented method to study discriminatory spatiotemporal features. The author conducted complete experimentations on publicly available CASME2 and SMIC datasets. Yildirim et al. [12] present a DL approach that interpreted variations in face into significant data trained through the Facial Expression Recognition data. Essential data is acquired by CV and assessed with the trained method. Wang et al. [13] introduce Haphazard Cuboids (HC) approach feature that generated target region by haphazard sampling approach and extracted micro-expression spatiotemporal attributes. HC has dual modules: temporal segment generation (TSG) and spatial patch generation (SPG).

Li et al. [14] modelled a deep local-holistic network approach for micro-expression detection. This presented technique has dual sub-networks a) Hierarchical Convolution RNN (HCRNN) that extracted the abundant and local spatiotemporal microexpression feature; b) Robust principal-component-analysis-related RNN (RPRNN), which extracts sparse and global features with micro-expression-specific representation. In [15], the authors devise a new DL technique named three-stream CNN (TSCNN) to deal with MER issue. The fundamental ideology of TSCNN is to study ME-discriminative attributes by merging facial, spatial, and temporal local region cues of the microexpression videos. Miao et al. [16] introduced a shallow CNN (SHCNN) structure with 3 layers to categorize micro-expressions and static expressions concurrently without big training data. Experiments are done on five open datasets: CASME II, FER2013, CASME, SAMM, and FERPlus.

The authors [17] presented an adaptive construction approach that depends on adaptive CNNs to build key-frame series for summarizing original ME videos that help to drop unnecessary frames and emphasize movements of apex frame. After, the novel key-frames are considered as inputs of the 2-stage learning approach. Abdullahi et al. [18] introduced state transition patterns depending on eye blinking, hands, and body motion features from real-life videos. For extracting spatial–temporal state transition patterns (STSTP) of face and hand poses, all video frames are denoted as per computed threshold values among neighbouring pixels.

3. The Proposed Model

In this article, we presented a novel ADDFM-ISSODL technique for an automated identification and classification of deceptive behaviour on facial microexpressions. The presented ADDFM-ISSODL technique examines the facial microexpressions effectively for the detection of deceptive behaviour. To accomplish this, the presented ADDFM-ISSODL technique operates on different stages: GF-based pre-processing, MobileNetv3 feature extraction, ISSO-based hyperparameter tuning, PNN classification, and GOA-based parameter optimization. Fig.1 denotes overall procedure of ADDFM-ISSODL technique.

DOI: https://doi.org/10.54216/IJAACI.050204
Received: August 11, 2023 Revised: December 13, 2023 Accepted: March 14, 2024

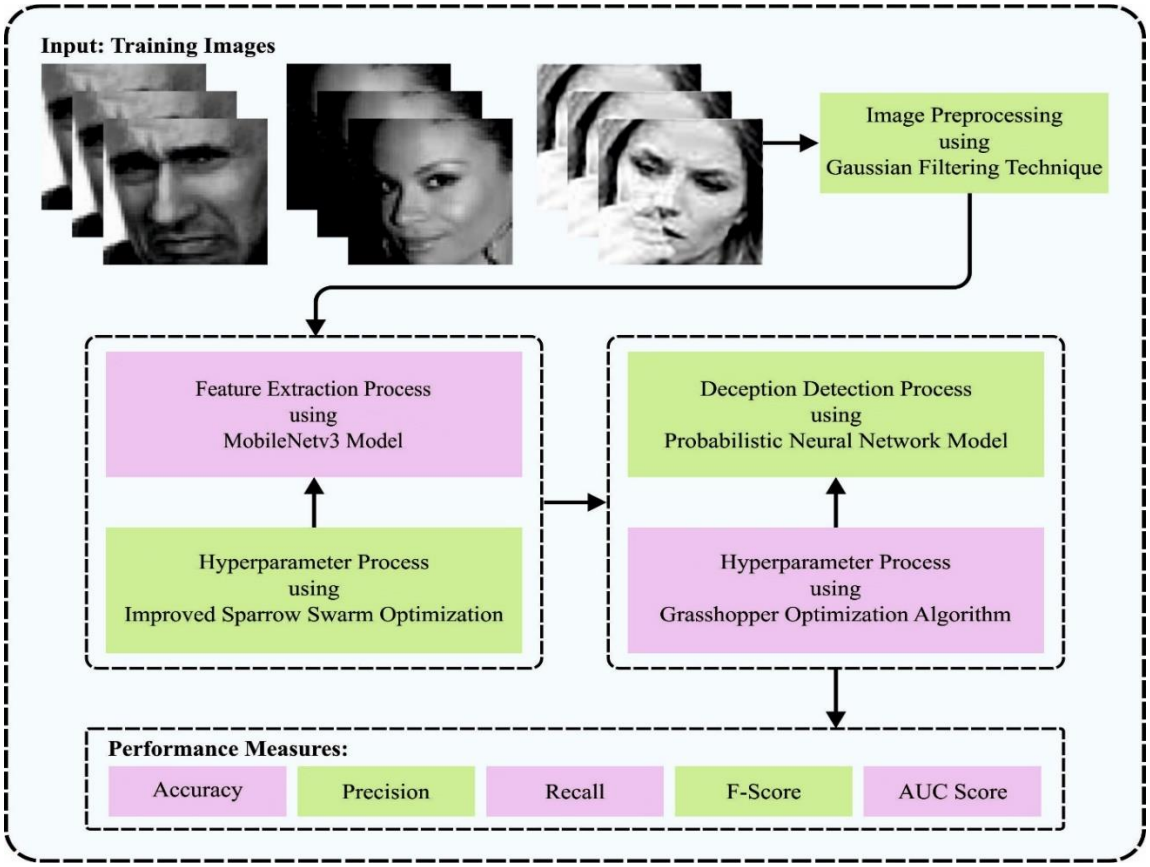

Fig. 1. Overall process of ADDFM-ISSODL algorithm

3.1. GF-based Pre-processing

For noise removal process, the GF approach was employed. It is used as an image processing method to reduce noise from an image [19]. It is named after the Gaussian distribution and it can be a probability distribution that contains a bell-shaped curve. The process includes convolving the image with a Gaussian filter kernel that can be a matrix of numbers that denote the weights allocated to adjacent pixels. From the Gaussian distribution, the values in the kernel can be derived, and they determine the quantity of smoothing implemented to the image. The kernel is cantered on the pixel being processed and the values in the kernel decline as the distance from the centre pixel surges.

3.2. Feature Extraction using MobileNetv3 Model

To derive a set of feature vectors from pre-processed images, MobileNetv3 technique exploited. Specific data about the execution of MobileNetV3 is utilized in this structure for WBC extraction feature [20]. This technique extracts the feature in a segmentation image which is offered as input. In many bottlenecks, blocks create the infrastructure of MobileNetV3. The remaining design is the most bottleneck block comprised in network. There exists just one track to feature extracted from typical bottleneck blocks that exchanged by dual feature extracted paths during this method named partial residual configuration. This architecture was utilized to lesser the computation cost of remaining structure.

A unique non-linearity in MobileNetV3 is called hard swish (hswish) that is superior form of sigmoid function. The h-swish non-linearity was utilized for reducing count of trained parameters and reducing difficulty of size and method that is written in Eq. (1).

$$h - swish\ (x) = x.\sigma(x) \quad (1)$$

$$\sigma(x) = \frac{\mathrm{Re}LU6(x+3)}{6} \quad (2)$$

DOI: https://doi.org/10.54216/IJAACI.050204
Received: August 11, 2023 Revised: December 13, 2023 Accepted: March 14, 2024

At this point, piece-wise linear hard analogy function referred to as $\sigma(x)$.

Primarily, the input image was provided as the network base layer which extracted primary features and forward them to bottleneck block. One portion can be exploited as mapping feature input for path1, and another can employ as mapping feature input for path2. An input mapping feature was evenly divided into 2 portions in path1. By the shortcut method, another path can be straightly connected to resultant of remaining learning part.

Likewise, in path2, the input mapping feature was equally divided into 2 portions. In this 11 Conv layer, 55 depth-wise Conv layer, and 1x1 Conv layer can execute to one portion. The resultant mapping feature 2 pathways can be linked utilizing the concatenation model. At last, the transition layer can be created to fuse concatenated mapping feature utilizing a 1x1 pointwise convolution kernel by batch normalization (BN) and ReLU or $h-swish$ activation function.

3.3. ISSO-based Hyperparameter Tuning

In this work, ISSO algorithm employed to optimally tune hyper parameter values of MobileNetv3 method. The SSO technique is a SI optimization method that stimulated by anti-predation and foraging activities of sparrow [21]. In this work, every individual in entire population can be divided into 3 dissimilar types: producer, scrounger, and scouter. The producer is accountable to determine foraging regions with high-quality food for entire populations and also has strong exploration ability, broad exploration space, and high energy reserves. Once the individual identifies the predator, the producer needs to lead others towards a safer region to prevent the attack of the predator. The updated position of producer is given below:

$$X_{i,j}^{t+1} = \begin{cases} X_{i,j}^{t} \cdot \exp\left(\dfrac{-i}{\alpha \cdot T_{\max}}\right) & R_2 < ST, \\ X_{i,j}^{t} + Q \cdot L, & R_2 \geq ST, \end{cases} \tag{3}$$

In Eq. (3), t indicates the current iteration amount, $X_{i,j}$ characterizes location of $i\text{-}th$ sparrows at $j\text{-}th$ dimensions ($j = 1,2, \ldots, \dim$), $\alpha \in (0,1]$ indicates the random integer, $T_{\max}$ shows maximal amount of iterations, $R_2 \in [0,1]$ and $ST \in [0.5,1]$ indicated alarm value and safety threshold, correspondingly, Q denotes random integer following standard distribution, L indicates the $1 \times \dim$ row vector and each element in it is 1.

The scrounger often follows producer to increase their energy reserves and attain high-quality food. Some scrounger monitors producer and competes for food. The updated position of scrounger is given below:

$$X_{i,j}^{t+1} = \begin{cases} Q \cdot exp\left(\dfrac{X_{worst}^{t} - X_{i,j}^{t}}{i^2}\right) & i > n/2, \\ X_{P}^{t+1} + \left|X_{i,j}^{t} - X_{P}^{t+1}\right| \cdot A^{+} \cdot L & \text{otherwise}, \end{cases} \tag{4}$$

In Eq. (4), n represent the amount of individuals in the population, A is a $1 \times \dim$ row vector, X_{worst}^{t} indicates the global worst location, X_{P}^{t+1} denotes the global optimum location, the element in it is randomly allocated 1 or -1, and $A^{+} = A^{T}(AA^{T})^{-1}$ denotes the MP inverse of A.

Some individual plays the role of scouter. They could identify threat modeled by predators and send out alerts to others to prevent. In this work, consider that this individual is accountable for 10-20% of the overall population, and their primary position is randomly allocated. The updating position of the scouters is shown below:

$$X_{i,j}^{t+1} = \begin{cases} X_{best}^{t} + \beta \cdot \left|X_{i,j}^{t} - X_{best}^{t}\right| & f_i > f_g, \\ X_{i,j}^{t} + K \cdot \left(\dfrac{\left|X_{i,j}^{t} - X_{worst}^{t}\right|}{(f_i - f_w) + \varepsilon}\right) & f_i = f_g \end{cases} \tag{5}$$

In Eq. (5), β, indicates step size control factor, which can be a random integer that follows standard distribution with a variance of 1 and mean value of 0; X_{best}^{t} denotes the present global optimum position; f_i shows the fitness value of present individual; $K \in [-1,1]$ denote the random value; ε denotes a smaller number to prevent denominator being 0; f_g and f_w represent the existing global optimum and worst fitness values, correspondingly.

DOI: https://doi.org/10.54216/IJAACI.050204
Received: August 11, 2023 Revised: December 13, 2023 Accepted: March 14, 2024

The ISSO approach was designed by the integration of a standard SSO system with a quantum evolutionary algorithm (QAE). Quantum computing (QC) is a new form of computing process which executes models compared to quantum method namely quantum entanglement, state superposition, and quantum measurement [22]. An essential unit of QC is qubit. The 2 essential states $|0>$ and $|1>$ process a qubit that depicted as a linear combination of these 2 essential states as below.

$$|Q>=\alpha|0>+\beta|1>. \quad (6)$$

$|\alpha|^2$ stands for probability of observed state $|0>$, $|\beta|^2$ denotes probability of observed state $|1>$, whereas $|\alpha|^2+|\beta|^2=1$. A quantum is made up of n qubits. Because of nature of quantum superposition, all quantum comprises 2^n possible values. An n-qubits quantum can be mentioned as:

$$\Psi=\sum_{x=0}^{2^n-1} C_x|x>, \sum_{x=0}^{2^n-1}|C_x|^2=1. \quad (7)$$

Quantum gates modify state of qubits such as rotation, NOT, and Hadamard gates. The rotation gate is determined as a mutation task to produce quanta process optimum solutions and lastly define global optimum solution. The rotation gate was decided as:

$$\begin{bmatrix}\alpha^d(t+1)\\ \beta^d(t+1)\end{bmatrix}=\begin{bmatrix}\cos(\triangle\theta^d) & -\sin(\triangle\theta^d)\\ \sin(\triangle\theta^d) & \cos(\triangle\theta^d)\end{bmatrix}\begin{bmatrix}\alpha^d(t)\\ \beta^d(t)\end{bmatrix} for\ d=1,2,\dots,n. \quad (8)$$

$\triangle\theta^d=\triangle\times S(\alpha^d,\beta^d)$, $\triangle\theta^d$ exemplifies the rotation angle of the qubit, whereas $\triangle$ and $S(\alpha^d,\beta^d)$ are dimensional and the direction of rotations correspondingly.

3.4. Deception Classification using PNN Model

For deception detection procedure, PNN technique employed. A NN comprises an interrelated layer of artificial neurons. The neuron in input layers are interconnected to neuron in hidden state were later interconnected to the resultant neuron [23]. The conventional NN is named a probabilistic neural network (PNN). PNN depends on Bayesian inference and is utilized for regression and classification errands like ranking search results or predicting prices. Fig. 2 represents the framework of PNN. This procedure is like how human learns grammar and language from the environment. The kernel implements the undeveloped process in PNN. It calculates the outcome probability. A kernel is considered a function which proceeds an input and maps it to other feature maps (dimensions). Then, kernel can be multiplied with each dot product with all the feature maps. The benefit of using PNN is that it can be quite insensitive to outliers and fast in training, generating more accurate outcomes than MLP networks.

PNN has output, input, pattern, and a summation layer; input flows over a sequence of "hidden" layers beforehand attaining an output level. When the input was transported in input to pattern layers through a pattern x_{ij} that can be the neuron vector, the outcome can be evaluated by the pattern layer.

$$\emptyset_{ij}(x)=\frac{1}{(2\pi)^{\frac{d}{2}}\sigma^d}\exp\left[\frac{(x-x_{ij})^T(x-x_{ij})}{2\sigma^2}\right] \quad (9)$$

In Eq. (9), x, and σ indicate the variable for smoothing and d denotes dimensional relevant to the pattern vector. The summation layer implements approximation of maximal probability of pattern x being considered in C_i classes. The output generated by neuron is averaged and combined based on specific class they belong to.

$$p_i(x)=\frac{1}{(2\pi)^d 2\sigma^d}\frac{1}{N_i}\sum_{j=1}^{Ni}\exp\left[\frac{(x-x_{ij})^T(x-x_{ij})}{2\sigma^2}\right] \quad (10)$$

$$\hat{C}(x)=\text{argmax}\{p_i(x)\}, i=1,2\dots,m \quad (11)$$

DOI: https://doi.org/10.54216/IJAACI.050204
Received: August 11, 2023 Revised: December 13, 2023 Accepted: March 14, 2024

Where m indicates the overall samples in a class. $C(x)$ Signifies the class estimation in terms of pattern x. the final output has been evaluated by Eq. (11) and depends on Bayes criterion.

Fig. 2. Structure of PNN

3.5. Parameter Tuning using GOA Algorithm

In the final phase, the GOA system was utilized for the optimum tuning of the PNN parameters. The grasshopper is an insect. They are regarded as a pest which causes crop and agriculture production [24]. Adult and larva are

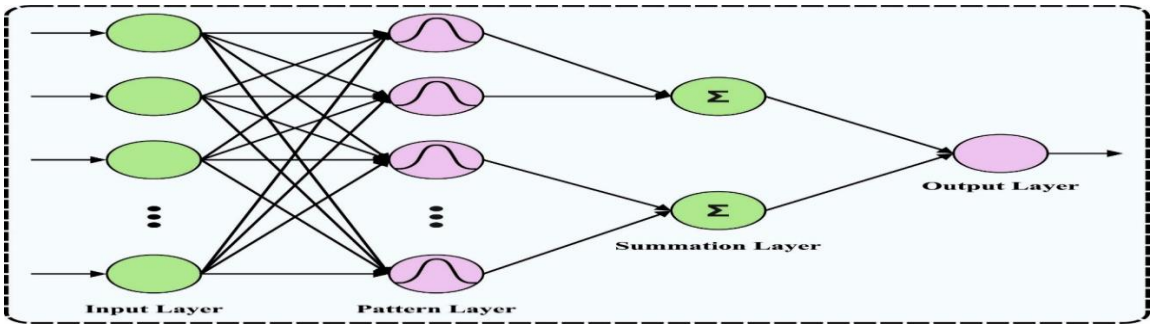

two major phases in the life cycle of grasshoppers. Grasshopper swarming is seen in both phases but with diverse behaviors. At the same time, an adult grasshopper forms a swarm in air and rapidly travels with great steps. The grasshopper movement can be mathematically modelled as follows:

$$X_i = S_i + G_i + A_i \tag{12}$$

$$S_i = \sum_{\substack{j-1 \\ j \neq i}}^{N} s\left(d_{ij}\right)\widehat{d_{ij}} \tag{13}$$

$$s(r) = fe^{-\frac{r}{l}} - e^{-r} \tag{14}$$

$$G_i = -g\widehat{e_g} \tag{15}$$

$$A_i = u\widehat{e_w} \tag{16}$$

Where l refers to the attractive length scale and f indicates the attraction intensity. X_i, S_i, G_i And A_i denote grasshopper location, social interaction force, gravitational force, and wind advection, correspondingly, d_{ij} and $\widehat{d_{ij}}$ represent distance and the unit vector in ith to jth grasshoppers, correspondingly. $s(r)$ Defines the social force between both grasshoppers, In Eq. (14), g shows gravitational constant and $\widehat{e_g}$ refers to the unity vector towards the middle of earth, u represents constant drift and $\widehat{e_w}$ shows the unity vector in wind direction. An improved form of formula to resolve the optimizer problem is given below

$$X_i^d = c\left(\sum_{\substack{j-1 \\ j \neq 1}}^{N} c\frac{ub_d - lb_d}{2} s\left(\left|x_j^d - x_i^d\right|\right)\frac{\chi_{j^-\chi_i}}{d_{ij}}\right) + \widehat{T_d} \tag{17}$$

In Eq. (16), lb_d and ub_d denote lower and upper boundaries at $the\ dth$ dimension, correspondingly. $\widehat{T_d}$ Shows value of $the\ dth$ dimension in target, and c indicates decreasing co-effectual to shrink repulsion, attraction and comfort region. To update parameter c the following formula is used.

$$c = c_{\max} - i\frac{c_{\max} - c_{\min}}{L} \tag{18}$$

In Eq. (17), L represents maximal amount number of iterations, $c_{\max}$ represents the maximal value, $c_{\min}$ refers to minimal value, and i shows index for existing iteration. Firstly, GOA method produces an arbitrary population of different groups of solutions, all of them having a set of bias function values.

DOI: https://doi.org/10.54216/IJAACI.050204
Received: August 11, 2023 Revised: December 13, 2023 Accepted: March 14, 2024

Fitness selection remains to be an important element in GOA approach. Solution encoding has been utilized to evaluate aptitude of candidate solutions. The accuracy value is key condition applied to suggest a fitness function.

$$Fitness = \max(P) \quad (19)$$

$$P = \frac{TP}{TP + FP} \quad (20)$$

TP represent true positive and FP means false positive value.

4. Performance Validation

In this section, performance validation of ADDFM-ISSODL approach was tested using the facial database, including 3500 instances under seven classes defined in Table 1. Fig. 3 signifies sample images.

Table 1: Details of database

Class	**No. Images**
Angry	500
Fear	500
Disgust	500
Happy	500
Surprise	500
Sad	500
Neutral	500
Total No. of Images	**3500**

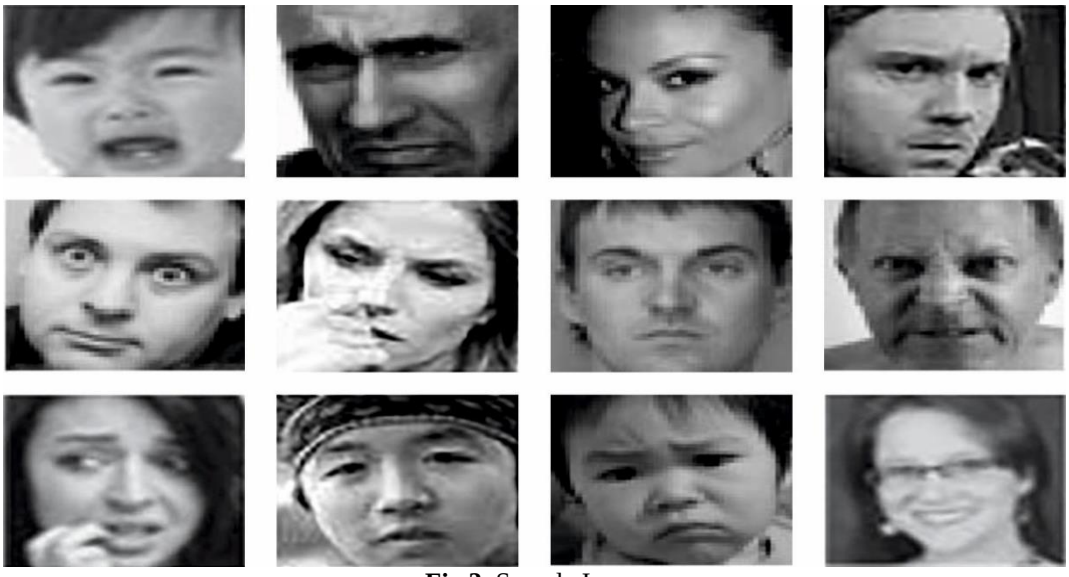

Fig.3. Sample Images

In Fig. 4, confusion matrices of ADDFM-ISSODL system clearly established. The figure reported that ADDFM-ISSODL technique detects different kinds of expressions accurately.

DOI: https://doi.org/10.54216/IJAACI.050204
Received: August 11, 2023 Revised: December 13, 2023 Accepted: March 14, 2024

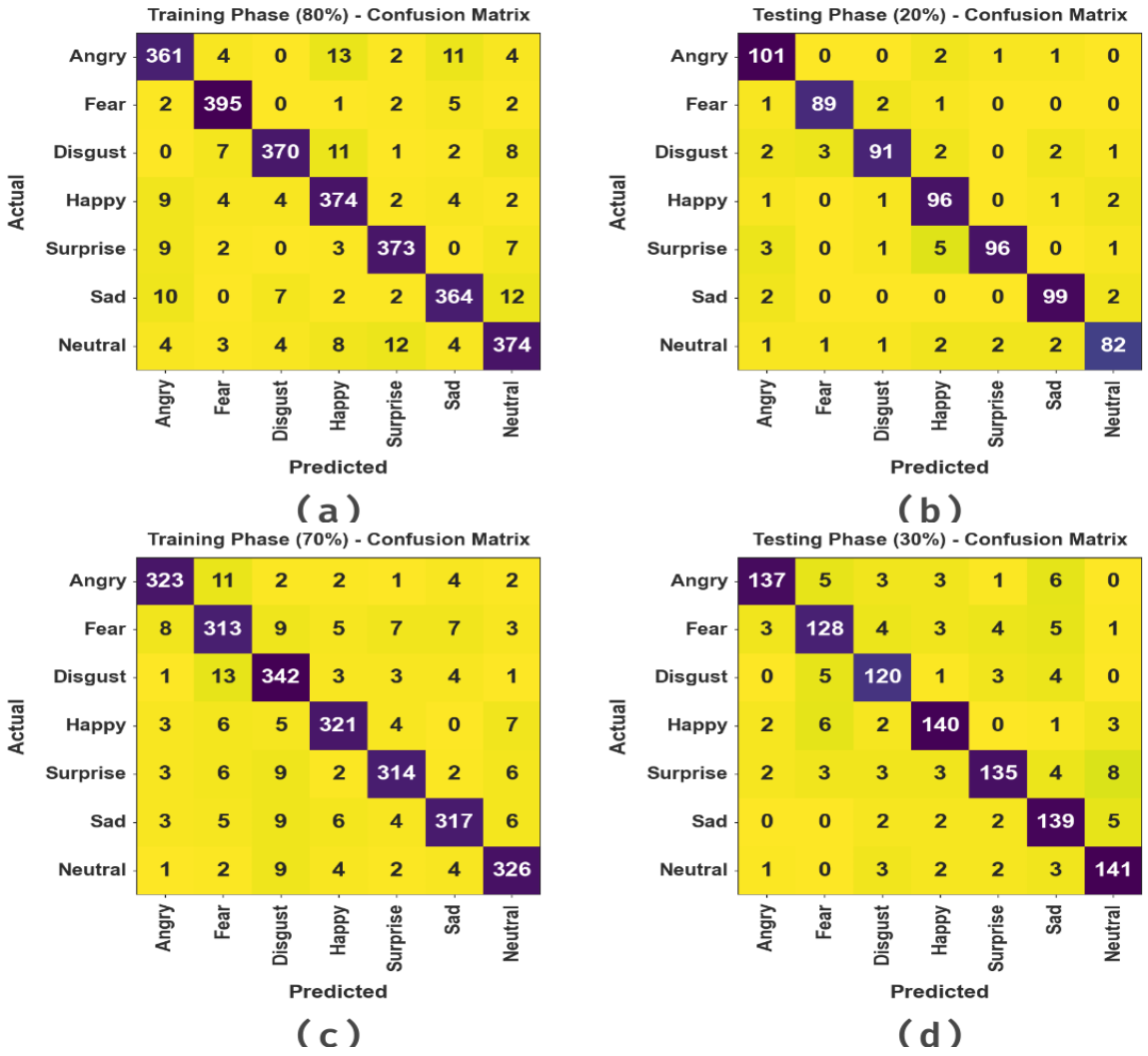

Fig. 4. Confusion matrices of ADDFM-ISSODL method (a-b) TRP/TSP of 80:20 and (c-d) TRP/TSP of 70:30

In Table 2, overall deception detection performance of ADDFM-ISSODL approach is clearly illustrated. Fig. 5 shows the brief deception detection results of ADDFM-ISSODL technique with 80:20 of TRP/TSP. The outcome indicates that ADDFM-ISSODL system identified various classes proficiently. For example, with 80% of TRP, the ADDFM-ISSODL methodology gains an average $accu_y$ of 98.07%, $prec_n$ of 93.27%, $reca_l$ of 93.24%, F_{score} of 93.25%, and AUC_{score} of 96.06%. Moreover, with 20% of TSP, the ADDFM-ISSODL methodology gains average $accu_y$ of 98.12%, $prec_n$ of 93.54%, $reca_l$ of 93.40%, F_{score} of 93.42%, and AUC_{score} of 96.15%.

Table 2 Deception detection outcome of ADDFM-ISSODL approach with distinct measures

Class	$Accu_y$	$Prec_n$	$Reca_l$	F_{score}	AUC_{score}
Training Phase (80%)					
Angry	97.57	91.39	91.39	91.39	94.99
Fear	98.86	95.18	97.05	96.11	98.11
Disgust	98.43	96.10	92.73	94.39	96.05
Happy	97.75	90.78	93.73	92.23	96.08
Surprise	98.50	94.67	94.67	94.67	96.90
Sad	97.89	93.33	91.69	92.50	95.30
Neutral	97.50	91.44	91.44	91.44	94.99
Average	**98.07**	**93.27**	**93.24**	**93.25**	**96.06**
Testing Phase (20%)					
Angry	98.00	90.99	96.19	93.52	97.25

DOI: https://doi.org/10.54216/IJAACI.050204
Received: August 11, 2023 Revised: December 13, 2023 Accepted: March 14, 2024

Fear	98.86	95.70	95.70	95.70	97.52
Disgust	97.86	94.79	90.10	92.39	94.63
Happy	97.57	88.89	95.05	91.87	96.52
Surprise	98.14	96.97	90.57	93.66	95.03
Sad	98.57	94.29	96.12	95.19	97.56
Neutral	97.86	93.18	90.11	91.62	94.56
Average	**98.12**	**93.54**	**93.40**	**93.42**	**96.15**
Training Phase (70%)					
Angry	98.33	94.44	93.62	94.03	96.36
Fear	96.65	87.92	88.92	88.42	93.44
Disgust	97.22	88.83	93.19	90.96	95.56
Happy	98.08	93.59	92.77	93.18	95.86
Surprise	98.00	93.73	91.81	92.76	95.41
Sad	97.80	93.79	90.57	92.15	94.79
Neutral	98.08	92.88	93.68	93.28	96.24
Average	**97.74**	**92.17**	**92.08**	**92.11**	**95.38**
Testing Phase (30%)					
Angry	97.52	94.48	88.39	91.33	93.75
Fear	96.29	87.07	86.49	86.78	92.19
Disgust	97.14	87.59	90.23	88.89	94.19
Happy	97.33	90.91	90.91	90.91	94.67
Surprise	96.67	91.84	85.44	88.52	92.05
Sad	96.76	85.80	92.67	89.10	95.06
Neutral	97.33	89.24	92.76	90.97	95.44
Average	**97.01**	**89.56**	**89.55**	**89.50**	**93.91**

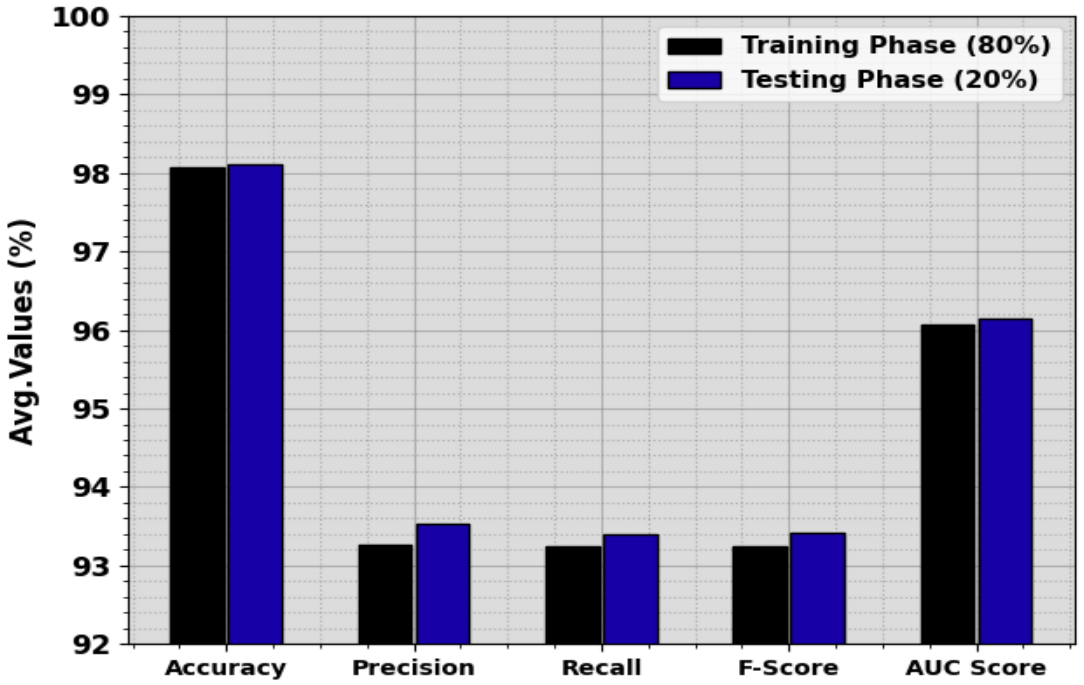

Fig. 5. Average analysis of ADDFM-ISSODL system on 80:20 of TRP/TSP

DOI: https://doi.org/10.54216/IJAACI.050204
Received: August 11, 2023 Revised: December 13, 2023 Accepted: March 14, 2024

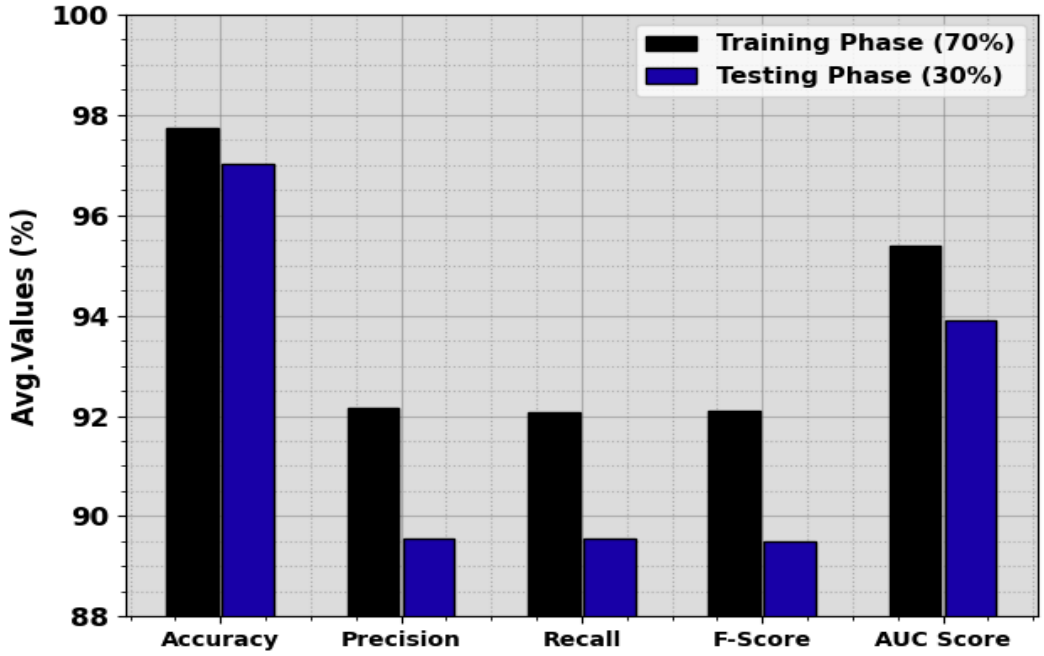

Fig. 6. Average analysis of ADDFM-ISSODL methodology on 70:30 of TRP/TSP

Fig. 6 exhibits the brief deception detection results of ADDFM-ISSODL technique with 70:30 of TRP/TSP. The outcome specify that ADDFM-ISSODL system identified distinct classes proficiently. For example, with 70% of TRP, ADDFM-ISSODL technique gains an average $accu_y$ of 97.74%, $prec_n$ of 92.17%, $reca_l$ of 92.08%, F_{score} of 92.11%, and AUC_{score} of 95.38%. Likewise, with 30% of TSP, ADDFM-ISSODL technique acquires average $accu_y$ of 97.01%, $prec_n$ of 89.56%, $reca_l$ of 89.55%, F_{score} of 89.50%, and AUC_{score} of 93.91%.

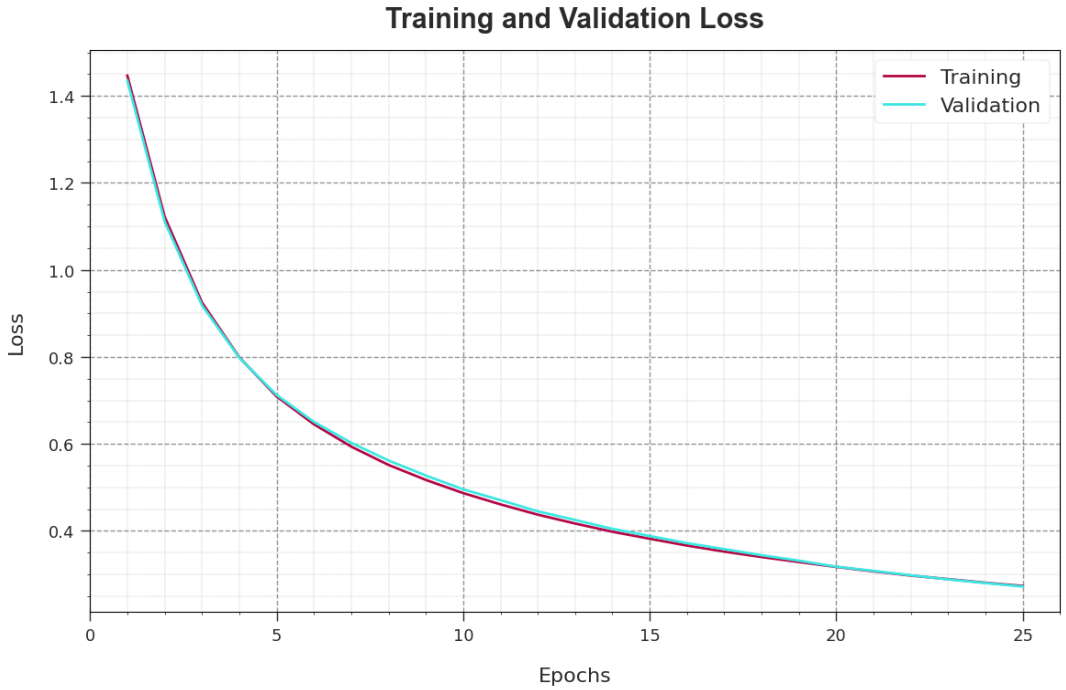

Fig. 7. Accuracy curve of the ADDFM-ISSODL approach

DOI: https://doi.org/10.54216/IJAACI.050204
Received: August 11, 2023 Revised: December 13, 2023 Accepted: March 14, 2024

Fig. 7 investigative $accu_y$ of ADDFM-ISSODL model on training and validation method on the test dataset. The result specifies that ADDFM-ISSODL technology attains higher $accu_y$ values over maximal epochs. As well, enhanced validation $accu_y$ over training $accu_y$ shows that ADDFM-ISSODL approach attains effectively on test dataset.

The loss study of the ADDFM-ISSODL methodology at time of training and validation discovered on test database in Fig. 8. The figure indicates that ADDFM-ISSODL technology gains near values of training and validation loss. The ADDFM-ISSODL system reaches capably the test database.

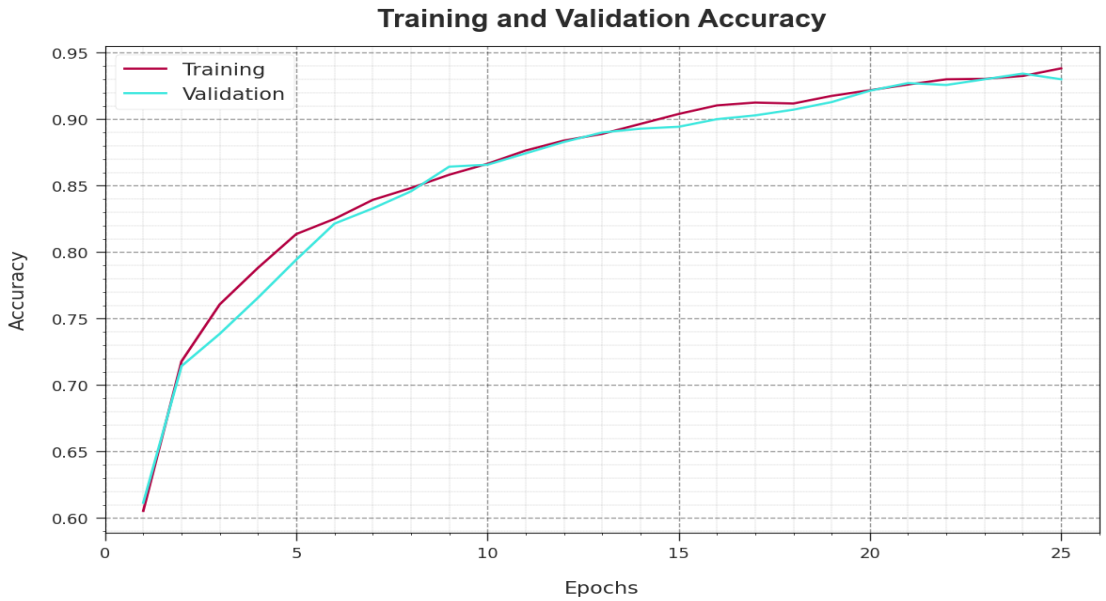

Fig. 8. Loss curve of the ADDFM-ISSODL approach

A brief precision-recall (PR) study of ADDFM-ISSODL technique is given on test dataset in Fig. 9. The result stated that ADDFM-ISSODL system outcomes in higher values of PR. Moreover, ADDFM-ISSODL approach attain higher PR values on 7 class labels.

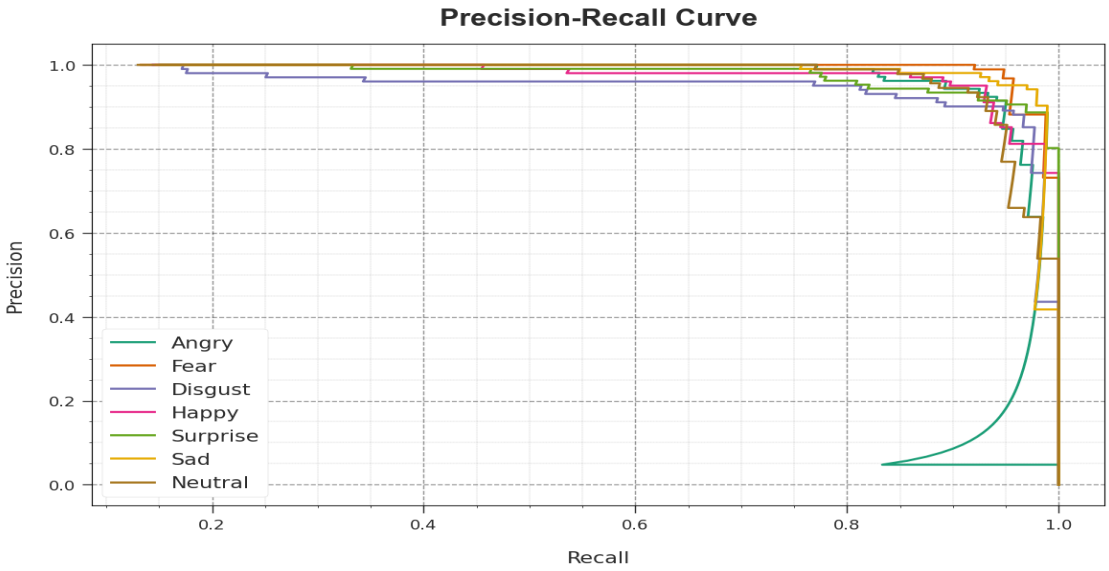

Fig. 9. PR curve of the ADDFM-ISSODL approach

DOI: https://doi.org/10.54216/IJAACI.050204
Received: August 11, 2023 Revised: December 13, 2023 Accepted: March 14, 2024

In Fig. 10, a ROC analysis of ADDFM-ISSODL methodology exposed on test database. The outcome defined that ADDFM-ISSODL technique improved ROC values. In addition, ADDFM-ISSODL method extend enhanced ROC values on 7 class labels.

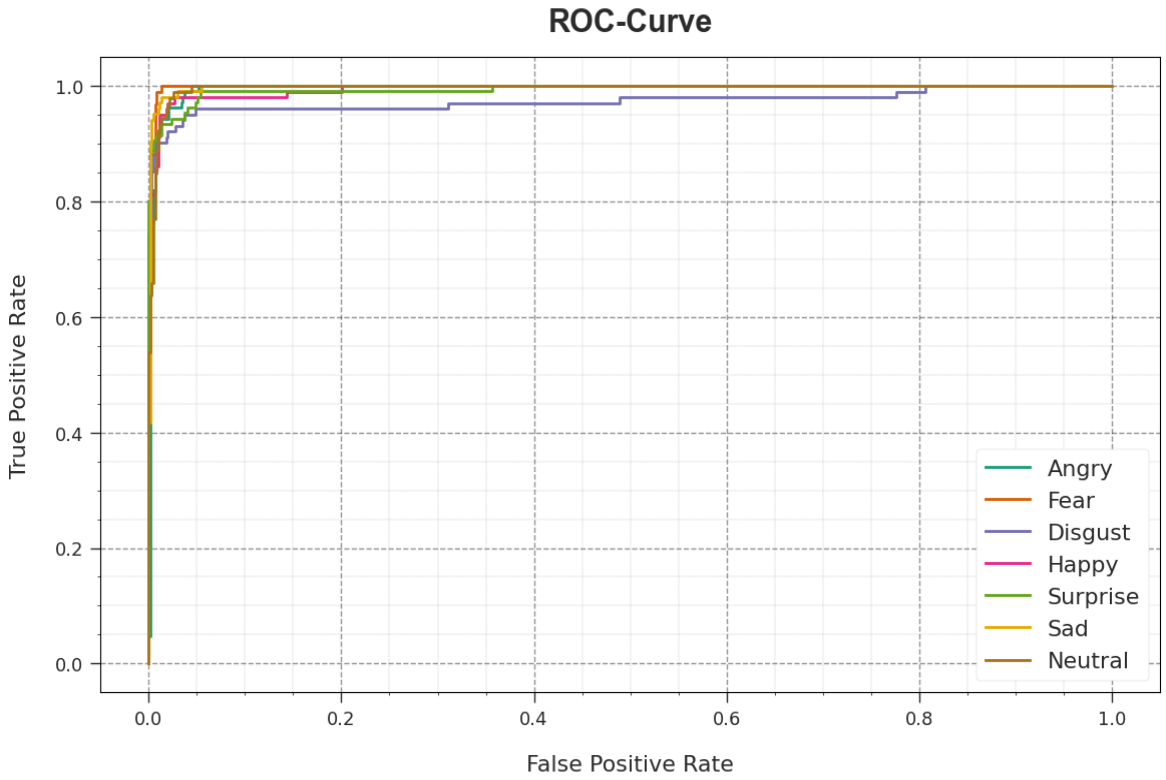

Fig. 10. ROC curve of the ADDFM-ISSODL approach

Table 3: $Accu_y$ outcome of ADDFM-ISSODL method with recent systems

Methods	**Accuracy (%)**
ADDFM-ISSODL	98.12
Facial Features-CNN	74.17
Spatial Features-CNN	96.00
Facial Features Unigrams-DT	75.00
Facial Features Unigrams-SVM	82.00
Facial Features-KNN	97.00

In Table 3 and Fig. 11, an overall comparative result of ADDFM-ISSODL model with recent techniques is given [12]. The outcome implied that the ADDFM-ISSODL technique obtains a higher $accu_y$ of 98.12%. Contrastingly, the existing facial features-CNN, spatial features-CNN, facial features unigrams-DT, facial features unigrams-SVM, and facial features-KNN models have obtained reduced $accu_y$ values of 74.17%, 96%, 75%, 82%, and 97% respectively. These results stated that the ADDFM-ISSODL technique gained enhanced deception detection performance.

DOI: https://doi.org/10.54216/IJAACI.050204
Received: August 11, 2023 Revised: December 13, 2023 Accepted: March 14, 2024

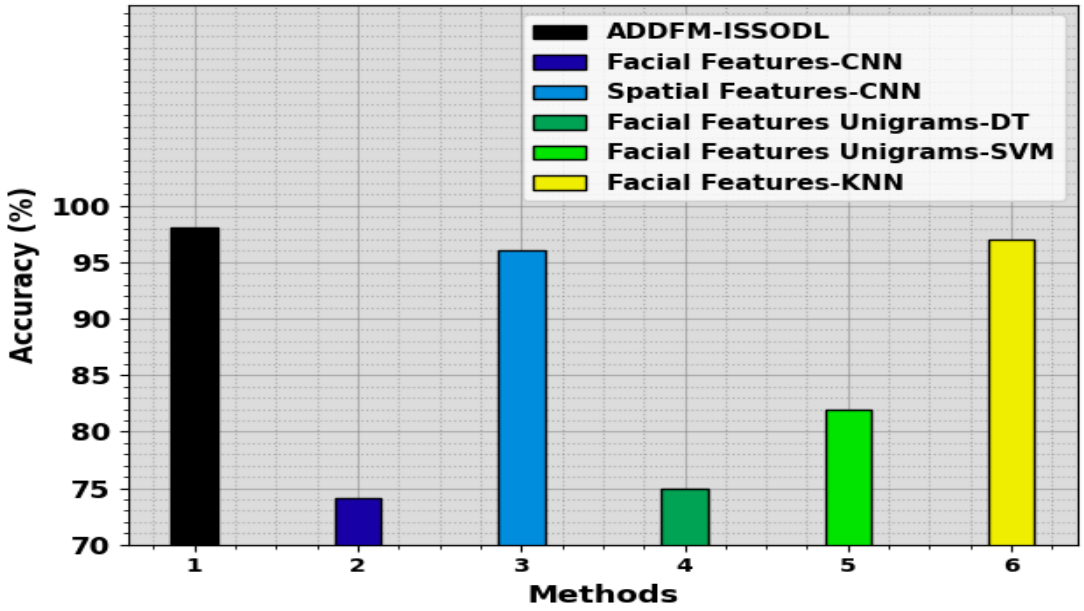

Fig. 11. $Accu_y$ Outcome of ADDFM-ISSODL approach with recent algorithms

5. Conclusion

In this paper, we projected a new ADDFM-ISSODL methodology for automated identification and classification of deceptive behaviour on facial microexpressions. The presented ADDFM-ISSODL technique examines the facial microexpressions effectively for the detection of deceptive behaviour. To accomplish this, the presented ADDFM-ISSODL technique operates on different stages: GF-based pre-processing, MobileNetv3 feature extraction, ISSO-based hyperparameter tuning, PNN classification, and GOA-based parameter optimization. The simulation outcomes of ADDFM-ISSODL method were tested using facial expression database. The performance validation stated improved results of ADDFM-ISSODL algorithm over other methods. In future works, deceptive detection efficiency of ADDFM-ISSODL technique was boosted by ensemble classification process.

References

[1] Tan, C., Ceballos, G., Kasabov, N. and Puthanmadam Subramaniyam, N., 2020. Fusionsense: Emotion classification using feature fusion of multimodal data and deep learning in a brain-inspired spiking neural network. *Sensors*, *20*(18), p.5328.

[2] He, X., Wu, X., Peng, J., Li, Q., Ma, X. and He, Y., 2023. *Bidirectional Cross-Scale Feature Fusion for Long Video Micro-Expression 3D Spotting Network* (No. 9818). EasyChair.

[3] Zhao, S., Tang, H., Liu, S., Zhang, Y., Wang, H., Xu, T., Chen, E. and Guan, C., 2022. ME-PLAN: A deep prototypical learning with local attention network for dynamic micro-expression recognition. *Neural Networks*, *153*, pp.427-443.

[4] Li, Z., Zhang, Y., Xing, H. and Chan, K.L., 2023. Facial Micro-Expression Recognition Using Double-Stream 3D Convolutional Neural Network with Domain Adaptation. *Sensors*, *23*(7), p.3577.

[5] Kumar, A.J.R., Theagarajan, R., Peraza, O. and Bhanu, B., 2019, June. CLASSIFICATION OF FACIAL MICRO-EXPRESSIONS USING MOTION MAGNIFIED EMOTION AVATAR IMAGES. In *CVPR Workshops* (pp. 12-20).

[6] Pan, H., Xie, L. and Wang, Z., 2022. Spatio-temporal convolutional emotional attention network for spotting macro-and micro-expression intervals in long video sequences. *Pattern Recognition Letters*, *162*, pp.89-96.

[7] Thuseethan, S., Rajasegarar, S. and Yearwood, J., 2023. Deep3DCANN: A Deep 3DCNN-ANN framework for spontaneous micro-expression recognition. *Information Sciences*, *630*, pp.341-355.

[8] Arora, T.K., Chaubey, P.K., Raman, M.S., Kumar, B., Nagesh, Y., Anjani, P.K., Ahmed, H.M., Hashmi, A., Balamuralitharan, S. and Debtera, B., 2022. Optimal facial feature-based emotional recognition using deep learning algorithm. *Computational Intelligence and Neuroscience: CIN*, *2022*.

DOI: https://doi.org/10.54216/IJAACI.050204
Received: August 11, 2023 Revised: December 13, 2023 Accepted: March 14, 2024

[9] Liu, N., Liu, X., Zhang, Z., Xu, X. and Chen, T., 2020, November. Offset or onset frame: A multi-stream convolutional neural network with capsulenet module for micro-expression recognition. In *2020 5th international conference on intelligent informatics and biomedical sciences (ICIIBMS)* (pp. 236-240). IEEE.
[10] Takalkar, M.A., Thuseethan, S., Rajasegarar, S., Chaczko, Z., Xu, M. and Yearwood, J., 2021. LGAttNet: Automatic micro-expression detection using dual-stream local and global attentions. *Knowledge-Based Systems*, *212*, p.106566.
[11] Wang, S., Guan, S., Lin, H., Huang, J., Long, F. and Yao, J., 2022. Micro-Expression Recognition Based on Optical Flow and PCANet+. *Sensors*, *22*(11), p.4296.
[12] Yildirim, S., Chimeumanu, M.S. and Rana, Z.A., 2023. The influence of micro-expressions on deception detection. *Multimedia Tools and Applications*, pp.1-19.
[13] Wang, G., Huang, S. and Dong, Z., 2022. Haphazard Cuboids Feature Extraction for Micro-Expression Recognition. *IEEE Access*, *10*, pp.110149-110162.
[14] Li, J., Wang, T. and Wang, S.J., 2022. Facial micro-expression recognition based on deep local-holistic network. *Applied Sciences*, *12*(9), p.4643.
[15] Li, K., Zong, Y., Song, B., Zhu, J., Shi, J., Zheng, W. and Zhao, L., 2019. Three-Stream Convolutional Neural Network for Micro-Expression Recognition. *Aust. J. Intell. Inf. Process. Syst.*, *15*(3), pp.41-48.
[16] Miao, S., Xu, H., Han, Z. and Zhu, Y., 2019. Recognizing facial expressions using a shallow convolutional neural network. *IEEE access*, *7*, pp.78000-78011.
[17] Zhao, S., Tao, H., Zhang, Y., Xu, T., Zhang, K., Hao, Z. and Chen, E., 2021. A two-stage 3D CNN based learning method for spontaneous micro-expression recognition. *Neurocomputing*, *448*, pp.276-289.
[18] Abdullahi, S.B., Bature, Z.A., Gabralla, L.A. and Chiroma, H., 2023. Lie Recognition with Multi-Modal Spatial–Temporal State Transition Patterns Based on Hybrid Convolutional Neural Network–Bidirectional Long Short-Term Memory. *Brain Sciences*, *13*(4), p.555.
[19] Chowdhury, D., Das, S.K., Nandy, S., Chakraborty, A., Goswami, R. and Chakraborty, A., 2019, March. An atomic technique for removal of gaussian noise from a noisy gray scale image using lowpass-convoluted gaussian filter. In *2019 International Conference on Opto-Electronics and Applied Optics (Optronix)* (pp. 1-6). IEEE.
[20] Rao, B.S.S. and Rao, B.S., 2023. An Effective WBC Segmentation and Classification Using MobilenetV3-ShufflenetV2 Based Deep Learning Framework. *IEEE Access*.
[21] Yang, Y., Tao, J., Zhou, J., Wang, J. and Guo, X., 2023. An Improved Sparrow Search Algorithm and Its Application in HIFU Sound Field. *Computational Intelligence and Neuroscience*, *2023*.
[22] Wang, D., Chen, H., Li, T., Wan, J. and Huang, Y., 2020. A novel quantum grasshopper optimization algorithm for feature selection. *International Journal of Approximate Reasoning*, *127*, pp.33-53.
[23] Alarfaj, F.K. and Khan, N.A., 2023. Enhancing the Performance of SQL Injection Attack Detection through Probabilistic Neural Networks. *Applied Sciences*, *13*(7), p.4365.
[24] Sherif, A. and Haci, H., 2023. A Novel Bio-Inspired Energy Optimization for Two-Tier Wireless Communication Networks: A Grasshopper Optimization Algorithm (GOA)-Based Approach. *Electronics*, *12*(5), p.1216.

DOI: https://doi.org/10.54216/IJAACI.050204
Received: August 11, 2023 Revised: December 13, 2023 Accepted: March 14, 2024